Exp Fluids (2012) 52:1319–1330
DOI 10.1007/s00348-011-1254-4

RESEARCH ARTICLE

Turbulence beneath finite amplitude water waves

J. F. Beyá · W. L. Peirson · M. L. Banner

Received: 8 June 2011 / Revised: 6 December 2011 / Accepted: 15 December 2011 / Published online: 4 January 2012
© Springer-Verlag 2012

Abstract Babanin and Haus (J Phys Oceanogr 39:2675–2679, 2009) recently presented evidence of near-surface turbulence generated below steep non-breaking deep-water waves. They proposed a threshold wave parameter $a^2\omega/\nu = 3{,}000$ for the spontaneous occurrence of turbulence beneath surface waves. This is in contrast to conventional understanding that irrotational wave theories provide a good approximation of non-wind-forced wave behaviour as validated by classical experiments. Many laboratory wave experiments were carried out in the early 1960s (e.g. Wiegel 1964). In those experiments, no evidence of turbulence was reported, and steep waves behaved as predicted by the high-order irrotational wave theories within the accuracy of the theories and experimental techniques at the time. This contribution describes flow visualisation experiments for steep non-breaking waves using conventional dye techniques in the wave boundary layer extending above the wave trough level. The measurements showed no evidence of turbulent mixing up to a value of $a^2\omega/\nu = 7{,}000$ at which breaking commenced in these experiments. These present findings are in accord with the conventional understandings of wave behaviour.

J. F. Beyá (✉)
Escuela de Ingeniería Civil Oceánica, Facultad de Ingeniería, Universidad de Valparaíso, Av. Brasil 1786 of. 30, Valparaíso, Chile
e-mail: jose.beya@uv.cl

J. F. Beyá · W. L. Peirson
Water Research Laboratory, School of Civil and Environmental Engineering, The University of New South Wales, Sydney, NSW 2052, Australia

M. L. Banner
School of Mathematics and Statistics, The University of New South Wales, Sydney, NSW 2052, Australia

1 Introduction

Correct understanding and representation of the interactions between turbulence and water waves is of fundamental importance to all aspects of air–sea interaction. This includes wave field development (e.g. Janssen 2004), constituent exchange (e.g. Jahne and Hausßecker 1998) and contaminant transport and dispersion (e.g. Burchard et al. 2008).

Conventional understanding is that the most common turbulence generation mechanisms at the air–ocean interface are wind-induced shear and surface wave breaking (Peregrine and Svendsen 1978). In both cases, turbulence is produced by shear adjacent to the surface and diffused downwards into the water column (Agrawal et al. 1992; Craig and Banner 1994).

However, quantifying the interaction between turbulence and surface water waves, in the field or laboratory, is a difficult exercise that requires decomposition of the near-surface velocity field into mean, oscillatory and turbulent components. Perhaps, the most advanced techniques were developed by Cheung and Street (1988) and Magnaudet and Thais (1995). They developed a suite of techniques to extract the turbulent velocity fluctuations from near-surface velocity motions. However, uncertainty remains regarding the coupling and energy fluxes between waves and turbulence (Jiang et al. 1998). The laser Doppler anemometry technique was adopted for these three investigations because of its low noise. Inherent instrument noise can compromise the characterisation of turbulence (e.g. Bradshaw 1971; Voulgaris and Trowbridge 1998; Nikora and Goring 1998; Chang and Liu 2000). A further difficulty is that the highest intensities of both the wave and turbulent motions are immediately adjacent to the moving interface and predominantly above the trough levels of the waves, a

region that is very difficult to probe with fixed point measurements (Siddiqui and Loewen 2007).

Because of these difficulties, there has been little direct quantitative evaluation of theoretical descriptions of wave–turbulence interactions (Teixeira and Belcher 2002; Ardhuin and Jenkins 2006).

Turbulent dissipation rates under wind-forced waves have been estimated from fixed point measurements in the presence of advective flow (Anis and Moum 1995; Terray et al. 1996; Gemmrich and Farmer 2004), and particle imaging measurements (Chang and Liu 1999; Sheng et al. 2000; Drazen and Melville 2009). The methods used rely on indirect computations of the dissipation rate via: (1) Kolmogorov-type spectrum fitting assuming isotropic, frozen turbulence, (2) turbulence scaling laws or (3) balancing of the turbulent kinetic energy equation.

In spite of the wide appreciation of the existence of turbulence immediately beneath the air–sea interface, conventional wave theories have been developed since Stokes (1847) that assume irrotational, inviscid flow and have been widely and successfully used to characterise wave-induced motions (CEM, p. II-1-2; SPM84; Tolman 2009 p. 7). Real waves are of finite amplitude, and this has motivated the development of higher-order Stokes wave representations. The validity of Stokes wave theories was extensively examined by Wiegel (1964) and included time exposure photographs of wave orbitals (p. 19), which supported the assumption of a non-turbulent condition within the subsurface flow.

Fenton (1985) developed a fifth-order Stokes theory that explicitly incorporates the role of a prevailing subsurface current. Swan (1990a) compared laser Doppler velocity measurements of unforced non-breaking monochromatic waves with Fenton (1985) and found excellent agreement. However, his velocity data did show fluctuations with an intensity of 0.02 ms^{-1}, which may be indicative of the presence of turbulence.

Longuet-Higgins (1953) extended Stokes' theory to explain the existence of bottom boundary layer transport in wave tank experiments by determining the vorticity generated within the viscous boundary layers adjacent to the water surface and the bed. The theory predicted an increase in the Stokes drift gradient near the surface that induces a second-order vorticity diffusing downward from the surface on a timescale $O(z^2/\nu)$, where z is the vertical coordinate with the origin at the still water level and ν is the fluid kinematic viscosity. It is to be noted that the existence of this second-order vorticity does not imply turbulent flow. These findings were verified by laboratory experiments (Longuet-Higgins 1960).

Recently, a laminar-turbulence transition wave amplitude Reynolds number parameter $a^2\omega/\nu$ (a is wave amplitude, and ω is wave angular frequency) has been proposed by Babanin and Haus (2009, hereafter BH2009), to account for the appearance of turbulence under non-breaking, monochromatic, deep-water laboratory waves ($\omega = 9.42$ $rads^{-1}$, water depth $d = 0.38$ m). The study by BH2009 was a refinement of earlier work by Babanin (2006).

The transition $a^2\omega/\nu$ was identified by BH2009 using Particle Image Velocimetry measurements immediately beneath the troughs of waves of a wide steepness range ($ak < 0.29$, k is the wave number). Dissipation rates greater than $10^{-3}m^2s^{-3}$ were reported for the sporadic appearance of a Kolmogorov-type spectrum leading to a proposed threshold value of $a^2\omega/\nu = 3{,}000$ for the occurrence of turbulence.

BH2009 can be compared with a theoretical analysis by Phillips (1961, also described in Kinsman 1984, p. 510). Using conventional turbulence scaling analysis and diffusion of vorticity, Phillips argued that wave-induced turbulence is governed by a Reynolds number defined as $R_W = \omega/(\nu k^2)$ and that under most oceanographical conditions, the largest disturbances are of third order in ak. Further, his theoretical estimate of the wave attenuation rate indicates an inverse proportional relation with R_W, showing that turbulence wave attenuation is a slow process compared with other third-order time-dependent properties of the wave field. To our knowledge, there has not been an independent empirical verification of the analysis described by Phillips.

If the present findings of BH2009 were validated, they would have significant and widespread implications for the entire air–sea interaction discipline. Is it possible that past experiments have failed to identify the presence of turbulence beneath waves due to the small scale of their experiments or lack of sensitivity of their instrumentation? Do freely propagating waves produce sufficient surface shear capable of creating turbulence? Is this claimed high level of turbulence under waves indicative of a fundamental flaw in conventional irrotational wave theory? The potential significance of the BH2009 findings prompted us to undertake a careful examination using techniques designed to detect the initiation of turbulence. These measurements included direct observations of wave motion, especially above the wave trough level, a region that has only been probed by a few investigators (Swan 1990a; Peirson 1997; Siddiqui and Loewen 2007). Before we proceed to describe the present experiments and consequent findings, it is useful to revisit previous measurements in the context of the parameter $a^2\omega/\nu$.

Figure 1 summarises relevant previous experimental studies. Careful flow visualisation experiments by Longuet-Higgins (1960) showed no evidence of turbulent motions but were undertaken at smaller values of $a^2\omega/\nu$ and may not be expected to detect such a transition in view of the proposed threshold parameter.

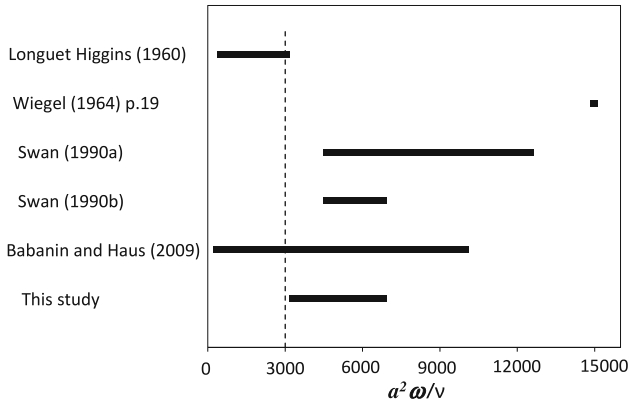

Fig. 1 Range of $a^2\omega/\nu$ for relevant experimental wave studies. Longuet-Higgins (1960) and Swan (1990a, b) studied waves in transitional depths. All other studies in this comparison investigated deep-water waves ($k_0 d > \pi$), k_0 = linear theory wave number. *Vertical dashed line* shows the transitional value in $a^2\omega/\nu$ as proposed by Babanin and Haus (2009)

Weigel's experiments were undertaken at larger scales ($a^2\omega/\nu \sim 15{,}000$), but it is possible that his visualisation techniques were not sufficiently sensitive to detect the presence of turbulence. As described earlier, Swan (1990a) did record fluctuations of 0.02 ms^{-1} in his measured velocities, but whether these are due to turbulence, instrument noise or variations in the wave field has not been determined. Consequently, these previous experiments neither confirm nor contradict the findings of BH2009.

In the present investigation, we have performed dye visualisation experiments of similar physical scale to BH2009.

2 Experimental method

2.1 Test facility

The present experiments were undertaken in a wave tank 30 m long, 0.6 m wide and 0.6 m total depth with glass sidewalls (Fig. 2). The wave tank was cleaned and filled with filtered tap water to a depth of 0.405 m.

Waves were generated with a programmable servo-controlled actuator driving a flexible plate cantilevered at a point near the tank floor. This form of wave generator was selected to minimise artefacts associated with wave generation by piston, wedge or flap paddles (Hughes 1993). A dissipative beach was located at the far end of the tank.

Prior to any measurements, floating material was removed from the surface by propagating steep waves along the tank and blowing the transported material onto and up the beach using a fan located near the far end of the tank.

To ensure that no residual turbulence diffused along the tank, fan and waves were stopped and a clean plastic sheet was placed on the water surface at the end of the tank in order to stop the slick returning to the cleaned surface, as used by Longuet-Higgins (1960). The wave tank was left to settle for 1 h, taking care that air and water currents were minimal.

A steep monochromatic wave train of angular frequency $\omega = 9.42$ rads^{-1} was generated for each test from a still water starting condition. Between tests, a solid screen was carefully placed in the middle of the tank for 5 min in order to dissipate any seiche motions in the tank. Then, the screen was carefully removed, and the next test was run when water movement was minimal.

Observations were undertaken at a distance of 5.25 m from the wave generator in order to match nominally the experimental conditions of BH2009.

2.2 Wave measurements

Wave height was measured at 5.25 m fetch using a capacitance probe. Data were recorded at 600 Hz sample rate by a National Instruments PCI-6225 data acquisition card installed in a conventional personal computer. The capacitance probe was calibrated carefully, yielding a linear response with a correlation coefficient greater than 0.998 and a noise level less than 0.05 mm.

The recorded water levels had their mean deducted and averaged over 15 points reducing the effective sample frequency to 40 Hz. Zero-crossing analysis was carried out to obtain the characteristic wave heights (H) and periods ($T = 2\pi/\omega$).

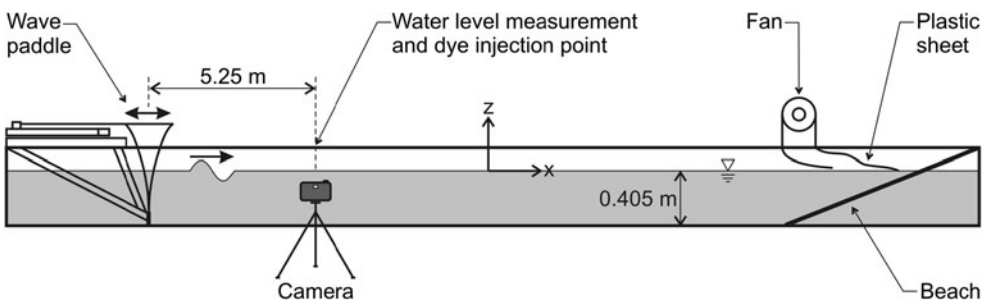

Fig. 2 Experimental set-up (not to scale)

For the dye experiments, wave trains propagating on still water were recorded after each visualisation measurement in order to avoid wave probe interference with the visualised flow.

2.3 Dye visualisation experiments

Dye visualisation techniques have been used to detect fluid velocities and turbulence since the birth of turbulence research over one hundred years ago (Reynolds 1883).

For this investigation, the flow visualisation was carried out by placing an approximately 2.5-mm-diameter magnesium permanganate crystal at the bottom of a slightly conical plastic tube. The tip of the plastic tube was rigidly supported, so that it just touched the water surface at the centre of the tank. Contact with the water caused the crystal inside the tube to dissolve, yielding a dense, intensely coloured descending plume of dye with a diameter of approximately 3 mm. Slight modulations in the dye dissolution created identifiable features in the developed dye line.

It was also possible to create dye lines in the presence of waves by dropping a small permanganate crystal at the crest of the passing wave. Larger crystals tended to fall too fast without allowing sufficient contact time to dissolve and generate a distinct line. Crystal shape and size selection was important since different shape crystals could create sinuous falling patterns. Round shape crystals of approximately 1 mm diameter created the most consistent lines although these were significantly thinner and harder to detect than the lines created in still water. Other dye injection techniques were tested without success. No further efforts were made to improve the quality of the lines in the presence of waves since the primary objective of this investigation was to visualise turbulence under the experimental conditions of BH2009, which involved waves propagating through quiescent water.

Appropriate lighting and diffusive screens were used to avoid reflections and to provide even illumination of the dye line. A Casio Exilim EX-F1 digital photo camera with a 35-mm lens was used to observe the dye line through the glass walls of the tank. The lens was carefully focused on the dye line with the camera set looking slightly upwards below the still water level in order to visualise the fluid underneath the water surface (Peirson 1997). High-definition video imagery (1,280 by 720 pixels) was captured at a rate of 30 frames per second.

The wave generator was started immediately after video recording commenced. The crystal and the tube were removed as soon as movement in the water surface was perceptible at the measurement point. Wave generation ceased after 30 waves had passed the measurement point. All dye experiments were undertaken over a period of 4 h during which the water temperature remained at 14.6 ± 0.2°C.

Once the suite of dye line imagery had been captured for all wave test conditions, the water level in the tank was raised by approximately 0.1 m and a square grid was immersed into the field of view at the centre of the tank for post-processing scaling and image rectification. Sample grid points were manually digitised from the grid image to create a transformation tensor and rectify all images, using the Matlab image processing toolbox (Matlab 2010).

Images of the evolving dye lines were extracted from the video at full resolution at selected times prior to rectification. The measurement resolution achieved by the system was 0.49 mm per pixel within the region of primary interest.

3 Results and discussion

3.1 Preliminary observations

More than 5 preliminary experiments were undertaken with steep monochromatic waves with $a^2\omega/\nu$ above the threshold specified by BH2009. On no occasion was rapid dispersion of the dye observed triggered by turbulence generated at the side walls or top of the tank (Figs. 3, 4). Yet, for steep, non-breaking waves of steepness $\xi = kH/2 > 0.22$, capillary ripples triggered by the side walls could be observed at the water surface (Fig. 5).

When the paddle was started from rest, the generated wave train contained an initial larger wave as shown in Fig. 6, which broke only for waves of steepness greater than $\xi = 0.24$ ($a^2\omega/\nu = 6{,}900$, Fig. 5). Five wave periods after the passage of this initial large wave, zero-crossing wave heights and periods showed that the subsequent wave train stabilised to an approximate monochromatic form. This dictated the start of video monitoring during each experiment. The duration of each experiment was then determined from the visual detectability of the dye line whose intensity decreased in time, primarily due to its continuous stretching by the Stokes drift.

It is important to note that for cases where $a^2\omega/\nu > 6{,}900$, the turbulence generated by the breaking of this initial wave (Fig. 5) induced rapid mixing of the dye line. This was observed to continue in bursts for several wave periods with the mixing deepening in time to a depth greater than the wave height, in qualitative agreement with Rapp and Melville (1990).

On the basis of these preliminary observations, three wave height cases were selected for detailed investigation with $a^2\omega/\nu > 3{,}000$, carefully avoiding the triggering of turbulence by wave breaking during initial wave field formation. The conditions of each experiment are summarised in Table 1.

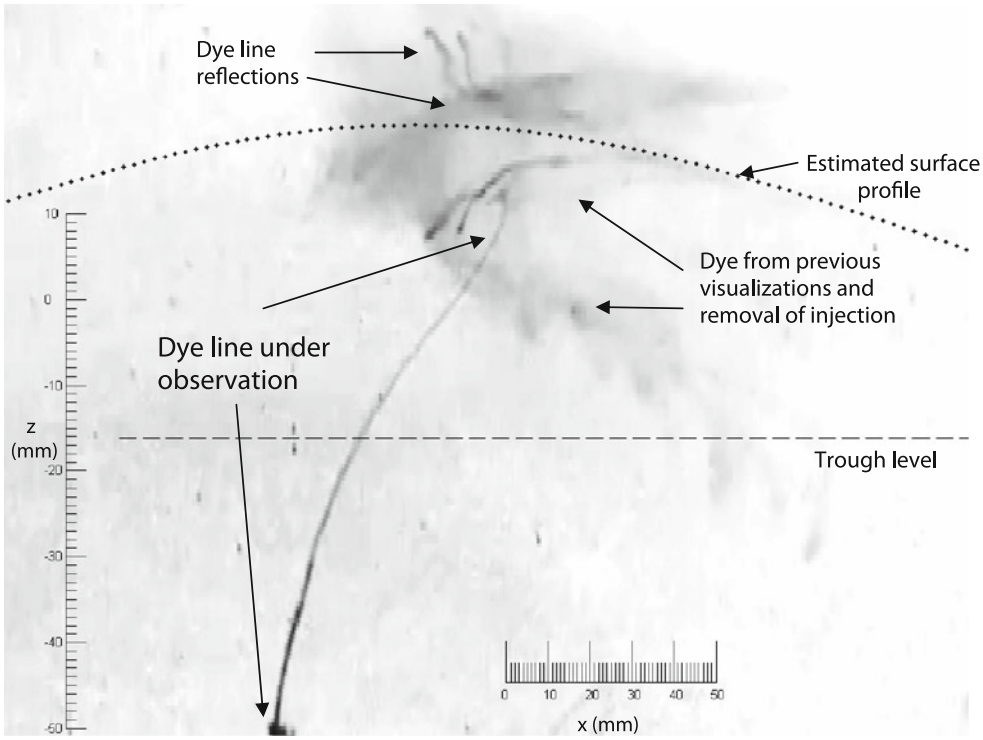

Fig. 3 Rectified and zoomed image of an evolving dye line at $t = 5T$ (Case 1) extracted from the video. The camera was set looking through the glass side wall below the still water level and looking slightly upwards. Image *horizontal* and *vertical* distortions are as indicated by the scales. Note the stretching (thinning) of dye line near the surface caused by the Stokes drift, with waves propagating from *left* to *right*. No turbulent dispersion of the dye line is observed. Some diffuse residual dye patches remain from previous visualisations and the removal of the injection tube. Dye features reflected in the water surface, as indicated, show the water surface position. The dotted line indicates the corresponding Fenton (1985) fifth-order theory water surface profile. The *dashed line* indicates the wave trough level. The vertical scale is aligned to the z axis, where $z = 0$ is the still water level

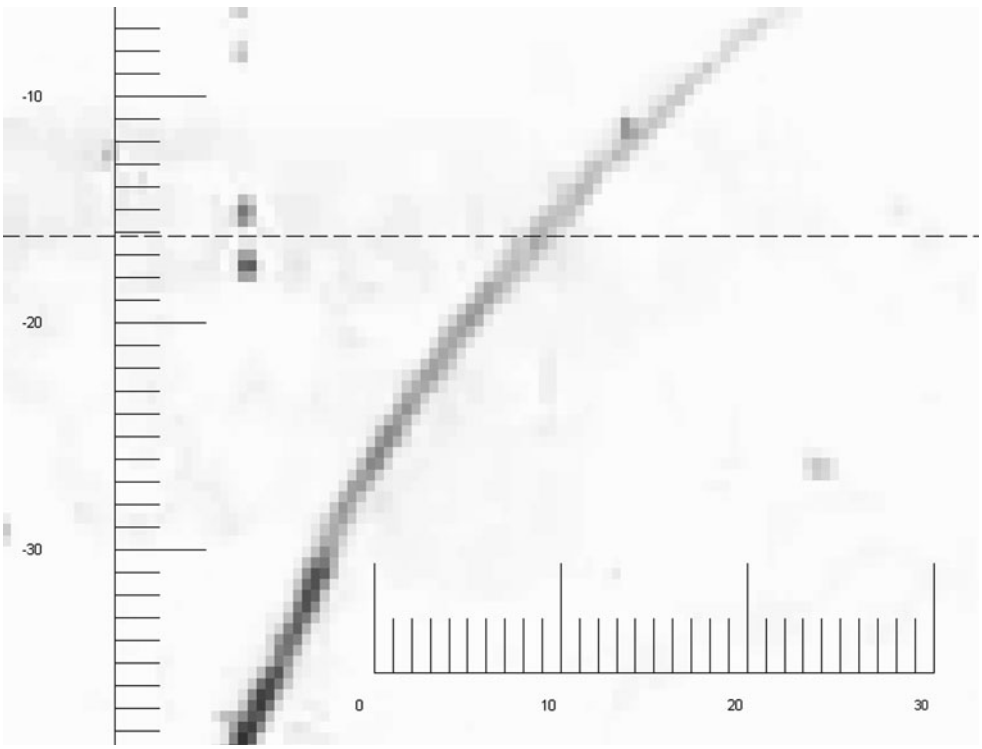

Fig. 4 Close-up of Fig. 3 ($t = 5T$, Case 1) showing no turbulent dispersion of the dye line in the vicinity of the trough level in contrast with the findings of Babanin and Haus (2009). Trough level is indicated by the dashed line. *Scales* indicate millimetres

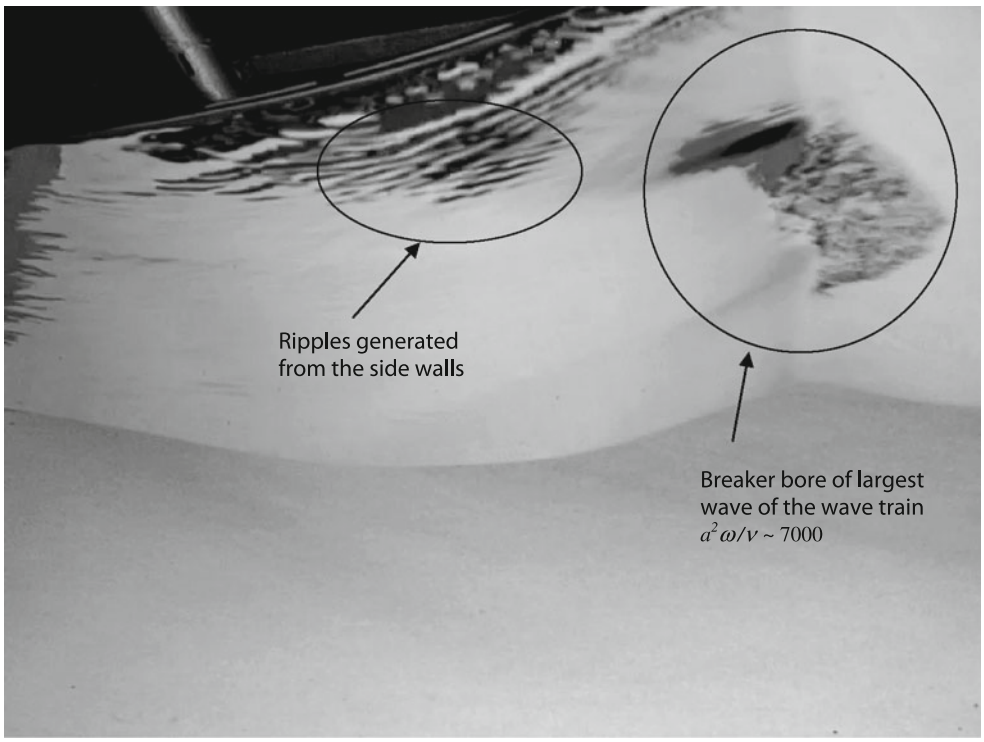

Fig. 5 Image showing the breaking (*right encircled area*) of the initial largest wave shown in Fig. 6 for a monochromatic wave train ($a^2\omega/\nu \sim 7{,}000$) propagating on still water. The image was taken from the tank side wall below the water surface near the tank floor and looking up towards the surface in an angle of approximately 60°. Capillary ripples triggered by side walls can also be observed at the water surface (*left encircled area*)

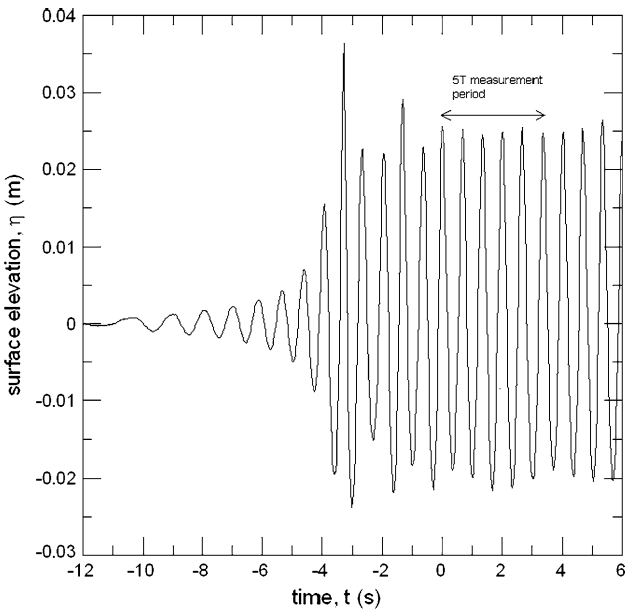

Fig. 6 Measured water elevation (η) time series, Case 2. Note start of the measurement period at $t = 0$, that is, when the wave train becomes stable five wave crests after the largest crest. Cases 1 and 3 showed similar behaviour. For all cases, H was calculated as the average of the zero-crossing values during the measurement period. $z = 0$ is the still water level

Table 1 Test cases of monochromatic wave trains generated from a still water start condition

Case	1	2	3
Half wave height, $H/2$ (mm)	18.7 ± 0.2	22.7 ± 0.1	26.9 ± 0.3
Wave steepness, ξ	0.17	0.21	0.24
$a^2\omega/v$	3,295	4,856	6,819

$\omega = 9.42$ rads^{-1}, $k_0 = \omega^2/g = 9.05$ radm^{-1}, $c_0 = \omega/k_0 = 1.041$ ms^{-1}, $d = 0.405$ m water depth

Although we analysed a time interval of $5T$ in detail, the total time from the initial perception of movement until the end of the measurement period is about $13T$. This duration is close to BH2009 measurement period. Further, we did not detect turbulent dye dispersion even after this period in any of the experiments undertaken.

In addition to the dye observations, corroborative ADV measurements were made over a much longer period of 2 min at 30 mm below the wave crest (at the same depth as the BH2009 PIV measurements). Wave generation continued for a much longer period of time, the instrument beam and head were immersed near the measurement point, and seeding had to be included in the water column.

The acquired time series and velocity spectra did not show any evidence of turbulent fluctuations and agreed with Fenton (1985) fifth-order wave theory. In the velocity spectra, higher wave harmonics were detected, and in the time series, no random fluctuations of the wave orbitals were observed.

3.2 Presence of turbulence

For each test case, the thickness of the dye line was measured at different depths at $t = 0$ and $t = 5T$ in order to quantify the turbulent mixing induced by the wave motion (Fig. 7). It is important to note that the observed dye line decreased in thickness and colour intensity near the surface due to the stretching caused by the Stokes drift as seen in Fig. 3. As additional qualitative supporting evidence for the absence of turbulence, a series of the original images taken at different times is included in Appendix for the three experimental cases listed in Table 1. No evidence of turbulent motions is observed.

The $5T$ time interval was chosen as the nominal monitoring period because for longer time intervals, the detection of the dye line close to the surface was difficult due to stretching of the dye line induced by the Stokes drift.

In the dye line experiments, the fact that the line could still be identified, that is, its thickness measured, indicates that no turbulent mixing had taken place (Reynolds 1883) in contrast with the conclusions of BH2009.

Vorticity as predicted and observed by Longuet-Higgins (1960) was not observed during these present dye visualisation experiments due to the short time available for vorticity to diffuse from the surface after initial wave generation.

BH2009 showed velocity spectra in which the turbulence integral length is of the order of $l = 0.005$ m (see their Fig. 1) and reported turbulent dissipation rates (ε) of $O(10^{-2}\mathrm{m}^2\mathrm{s}^{-3})$ for $a^2\omega/\nu > 3{,}000$ (see their Fig. 2). This level of ε is comparable to the highest near-surface values observed under strong wind forcing in Lake Ontario (Terray et al. 1996). For an ε value of $O(10^{-3}\mathrm{m}^2\mathrm{s}^{-3})$, turbulent velocity fluctuations (u') must be of $O(0.02\ \mathrm{ms}^{-1})$ according to:

$$\varepsilon = A\frac{u'^3}{l} \tag{1}$$

where ε is the turbulent kinetic energy dissipation rate per unit volume, u' is the intensity of the velocity fluctuations, l is the turbulence integral length, and A is a constant of O(1) (Tennekes and Lumley 1972, p. 20), valid for isotropic turbulence that develops a inertial sub-range. This velocity value is significant, being about 10% of the maximum orbital velocity near the surface but smaller than the stated accuracy of their PIV system ($\pm 0.03\ \mathrm{ms}^{-1}$, see

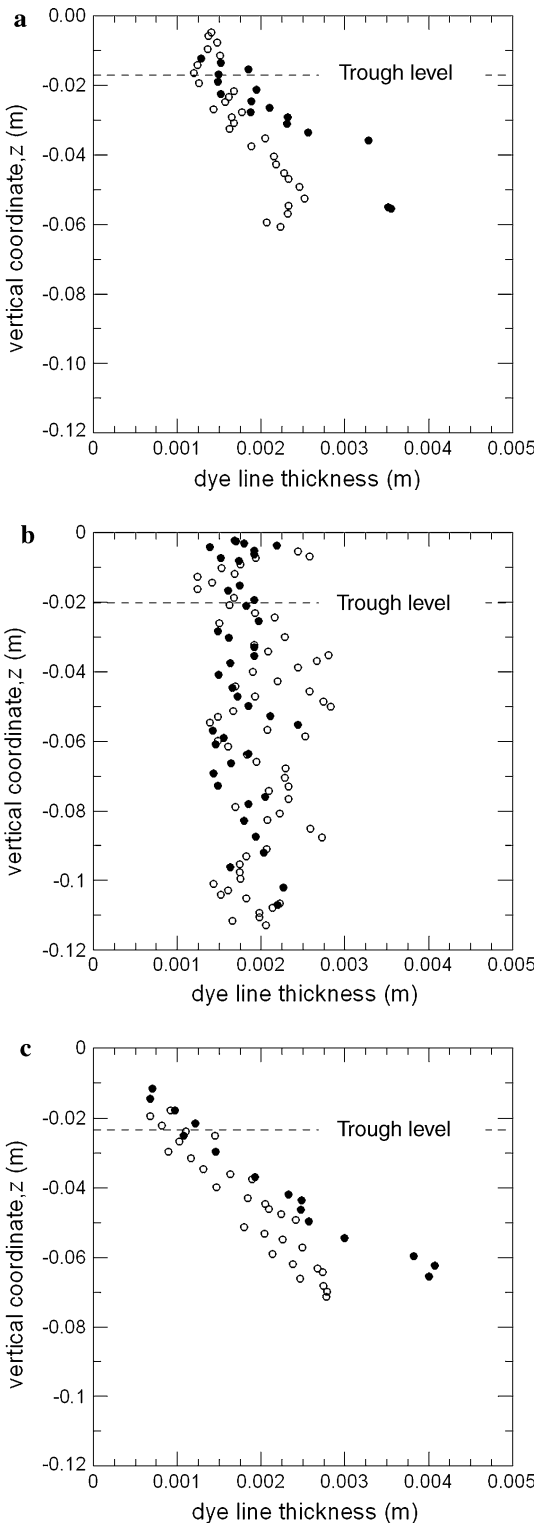

Fig. 7 Vertical profile of dye line thickness at time ($t = 0$) (*solid circles*) and ($t = 5T$) (*hollow circles*). **a** Case 1, **b** Case 2, **c** Case 3. *Horizontal dashed lines* indicate estimated fifth-order theory trough levels. $z = 0$ is the still water level

their p. 2677). The present experiments showed no turbulent velocity fluctuations with a detection limit of approximately 0.3 mms^{-1} (Figs. 4, 7). This detection limit was quantified by the maximum standard error of the least squares fitting of sinusoidal velocity functions to dye measurements of orbital velocities. Dye line trackable features were digitised and the measured instantaneous velocities obtained by dividing the displacements by the time step.

The BH2009 conclusions that turbulence is spontaneously generated beneath water waves in the absence of wind forcing and active breaking could be due to their having neglected at least one of the following factors in their experiments:

1. BH2009 does not specify the type of wave paddle they used. An inappropriate wave paddle may cause the generation of artefacts that could have an effect in the wave velocity field (Hughes 1993, p. 368). While we believe it is unlikely that paddle artefacts would trigger strong turbulence 5 m from the paddle, artefacts in the wave field can cause group non-linearities that can cause localised micro-breaking which is transitory and difficult to observe but can directly generate subsurface turbulence.
2. We have detected that when a monochromatic wave train is generated from a still water start and under similar experimental conditions than of BH2009, there is a larger wave that breaks when $a^2\omega/v$ is greater than 7,000 as shown in Fig. 5. They present results for waves of $a^2\omega/v$ greater than 7,000, but they do not reference to breaking events. It is possible that the breaking of this first wave went unnoticed.
3. BH2009 mentions that the accuracy of their PIV system is 0.03 ms^{-1} (BH2009, p. 2677, first paragraph, last line), which is greater than the anticipated level of turbulence intensity O(0.02 ms^{-1}) according to the scaling law shown in Eq. 1 with $A = 1$. On the basis of their stated figures, it is difficult to see how their PIV measurements could have sufficient accuracy to resolve their stated turbulence levels.
4. BH2009 shows an example of a velocity spectrum from where they infer the occurrence of turbulence by fitting a $-5/3$ slope within the high frequencies range. The appearance of this type of spectrum was said to be intermittent. Given the limitations of their PIV system, careful analysis would be required to apply turbulence theories derived for isotropic, steady flow such as the $-5/3$ slope Kolmogorov energy cascade to unsteady, anisotropic flows. It has been shown by Magnaudet and Thais (1995) and Cheung and Street (1988) that correctly filtering the non-turbulent components is crucial when attempting to adequately characterise turbulence in wavy flows. Chang and Liu (2000) showed that PIV data could wrongly be interpreted as turbulence, an artefact they named pseudo-turbulence. BH2009 does not present any consideration of these effects nor how they were eliminated from their measurements.
5. Steep waves are non-linear as their velocity field and surface elevation cannot be represented by a single Fourier mode. This leads to the appearance of higher harmonics in the wave amplitude and wave velocity energy spectra, which may bias turbulence measurements inferred from velocity spectra measured below such non-linear waves. The BH2009 velocity spectra from which turbulent dissipation rates were derived may have been influenced by this effect.

4 Conclusions and recommendations

We have reported unique high-resolution dye measurements of near-surface motion beneath steep gravity waves in the absence of breaking and wind forcing. These dye measurements were carried out under similar experimental conditions to BH2009 and above their proposed threshold of $a^2\omega/v = 3{,}000$ up to a value of approximately $a^2\omega/v = 7{,}000$. The present results support the conventional understanding of an absence of turbulence beneath two-dimensional, freely propagating, unforced, non-breaking waves. This is in contrast with the findings of BH2009 who reported turbulence levels comparable to field measurements under strong winds (e.g. Terray et al. 1996) when a non-dimensional parameter $a^2\omega/v$ exceeds 3,000.

Appendix

See Figs. 8, 9 and 10.

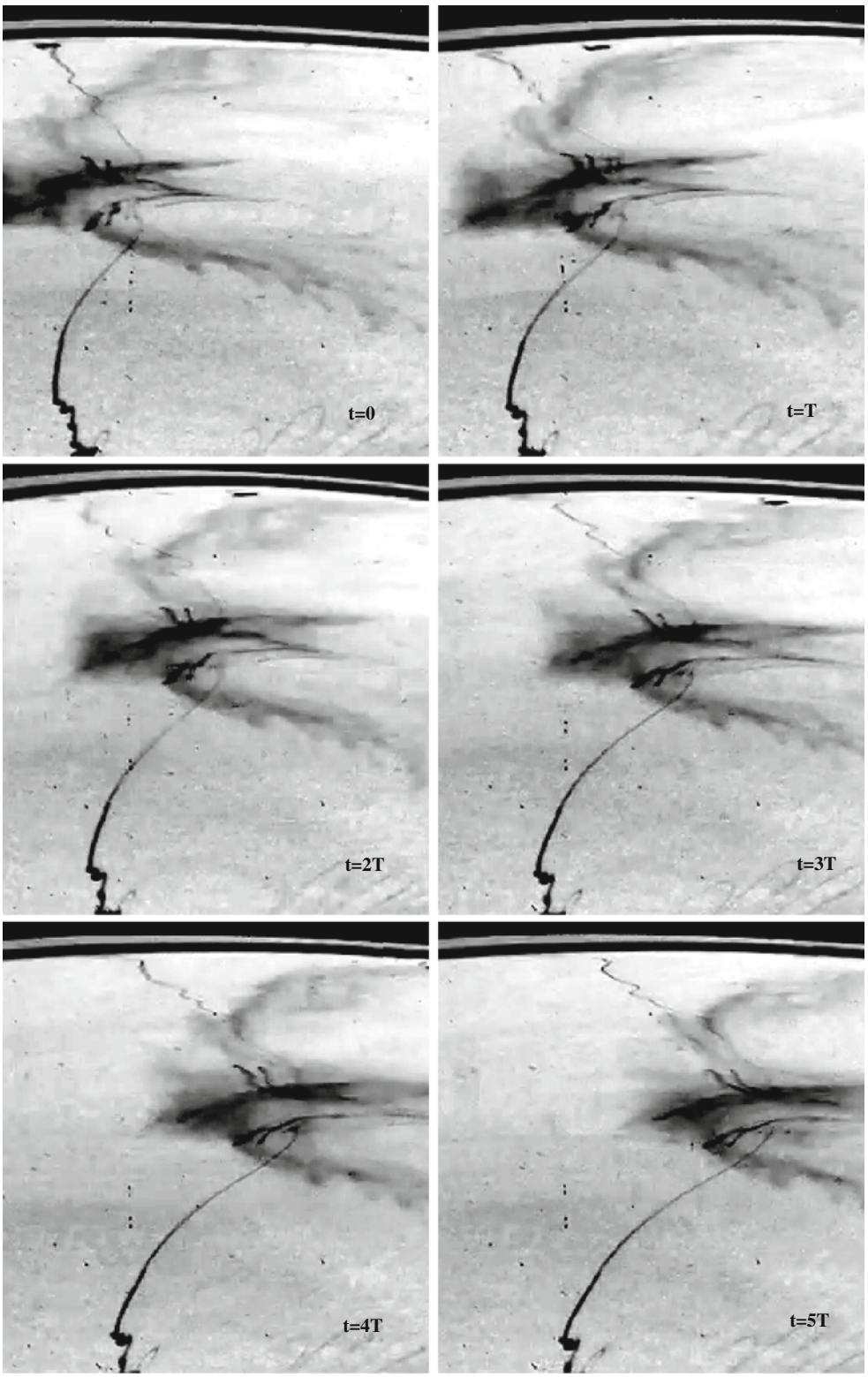

Fig. 8 Image sequence from $t = 0$ to $t = 5T$, Case 1, No zoom, no rectification, no image geometric distortion, contrast and brightness adjusted

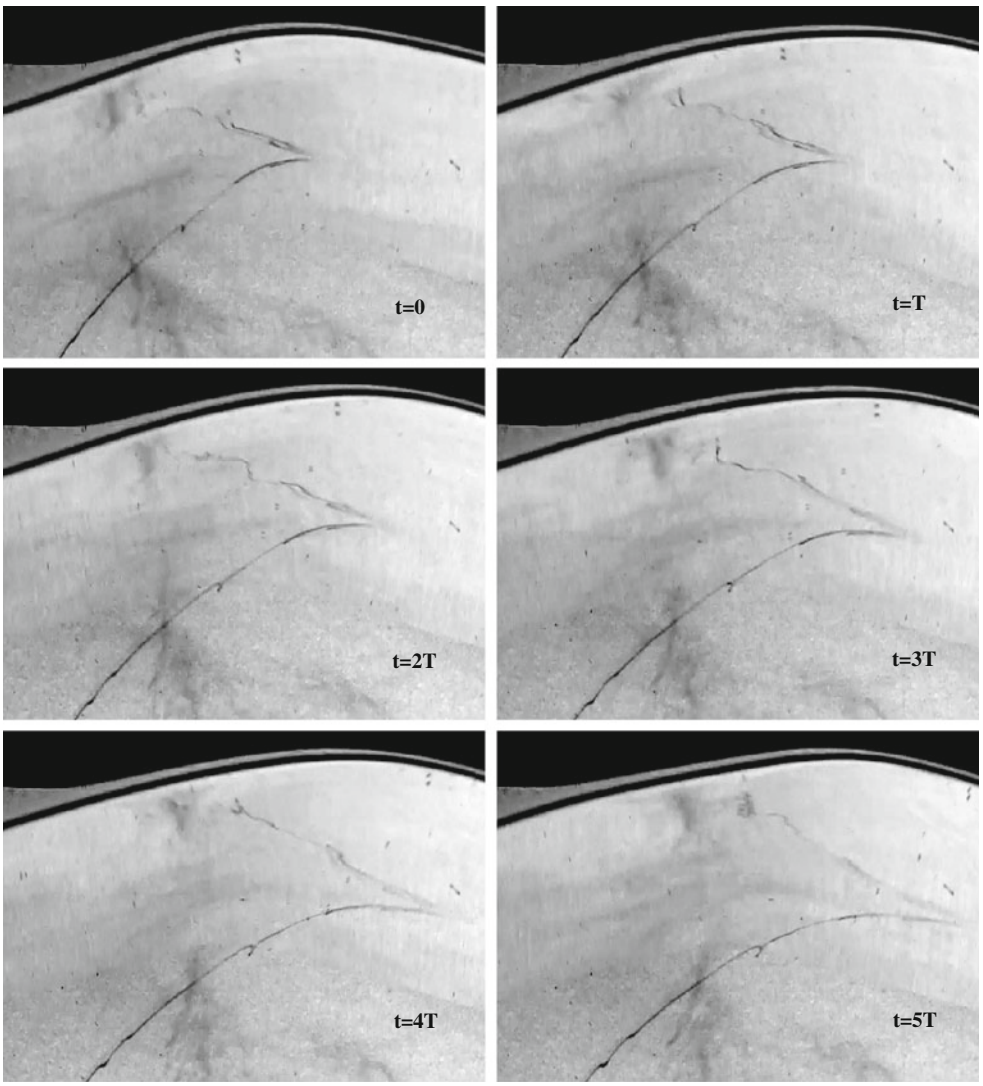

Fig. 9 Image sequence from $t = 0$ to $t = 5T$, Case 2, zoomed out images, no rectification, images with geometric distortion (H41%:V65%), contrast and brightness adjusted

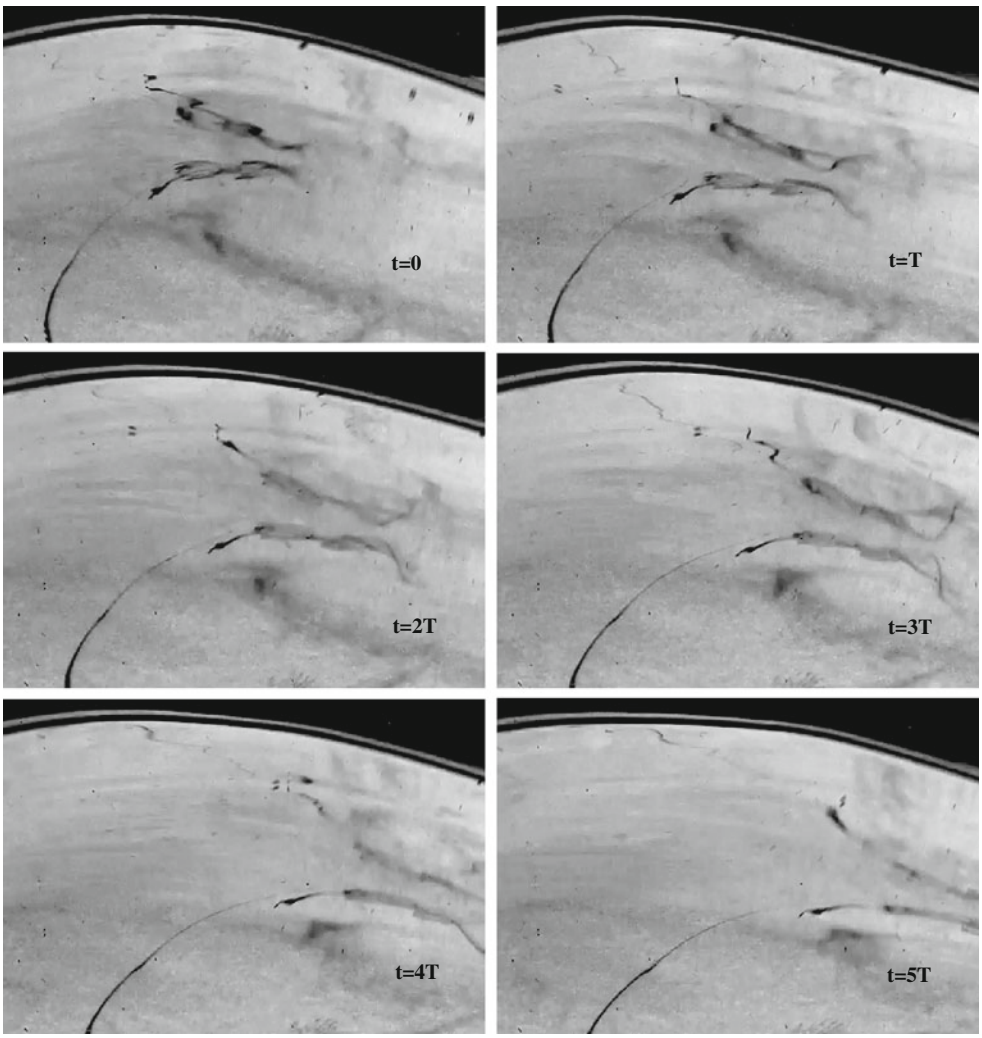

Fig. 10 Image sequence from $t = 0$ to t = 5*T*, Case 3, zoomed out images, no rectification, images with geometric distortion (H51%:V60%), contrast and brightness adjusted

References

Agrawal Y, Terray E, Donelan M, Hwang P, Williams A, Drennan W, Kahma K, Kitaigorodskii S (1992) Enhanced dissipation of kinetic energy beneath surface waves. Nature 359:219–220

Anis A, Moum J (1995) Surface wave-turbulence interaction: Scaling ε (z) near the sea surface. J Phys Oceanogr 25: 2025–2045

Ardhuin F, Jenkins A (2006) On the interaction of surface waves and upper ocean turbulence. J Phys Oceanogr 36:551–557

Babanin A (2006) On a wave-induced turbulence and a wave-mixed upper ocean layer. J Phys Oceanogr L20605(33):1–6

Babanin A, Haus B (2009) On the existence of water turbulence induced by non-breaking surface waves. J Phys Oceanogr 39: 2675–2679 (Notes and Correspondence)

Bradshaw P (1971) An introduction to turbulence and its measurement. Pergamon Press, First edition

Burchard H, Craig P, Gemmrich J, van Haren H, Mathieu P, Meier H, Smith W, Prandke H, Rippeth T, Skyllingstad E, Smyth W, Welsh D, Wijesekera H (2008) Observational and numerical modeling methods for quantifying coastal ocean turbulence and mixing. Prog Oceanogr 76–4:399–442

Chang K, Liu P (1999) Experimental investigation of turbulence generated by breaking waves in water of intermediate depth. Phys Fluids 11–11:3390–3400

Chang K, Liu P (2000) Pseudo turbulence in PIV breaking-wave measurements. Exp Fluids 29:331–338

Cheung T, Street R (1988) The turbulent layer in the water at an air-water interface. J Fluid Mech 194:133–151

CEM, Coastal Engineering Manual (2008) US Army Corps of Engineers, Washington, DC (in 6 volumes)

Craig P, Banner M (1994) Modelling wave-enhanced turbulence in the ocean surface layer. J Phys Oceanogr 24:2546–2559

Drazen D, Melville W (2009) Turbulence and mixing in unsteady breaking surface waves. J Fluid Mech 628:85–119

Fenton J (1985) A fifth-order stokes theory for steady waves. J Waterw Port Coast Ocean Eng 111(2):216–234

Gemmrich J, Farmer D (2004) Near-surface turbulence in the presence of breaking waves. J Phys Oceanogr 34:1067–1086

Hughes S (1993) Physical models and laboratory techniques in coastal engineering. Advanced Series on Ocean Eng, vol 7. World Scientific Publications, Singapore

Jahne B, Haußecker H (1998) Air-water gas exchange. Annu Rev Fluid Mech 30:443–468

Janssen P (2004) The interaction of ocean waves and wind. Cambridge University Press, Cambridge

Jiang L, Perlin M, Shultz W (1998) Period tripling and energy dissipation of breaking standing waves. J Fluid Mech 369: 273–299

Kinsman B (1984) Wind waves, their generation and propagation on the ocean surface. Dover publications, Inc., New York

Longuet-Higgins M (1953) Mass transport in water waves. Phil Trans R Soc Lond A 245:535–581

Longuet-Higgins M (1960) Mass transport in the boundary layer at a free oscillating surface. J Fluid Mech 8:293–306

Magnaudet J, Thais L (1995) Orbital rotational motion and turbulence below laboratory wind water waves. J Geophys Res 100(C1): 757–771

Matlab® R (2010a)

Nikora V, Goring D (1998) ADV Measurements of turbulence: Can we improve their interpretation? JHydr Eng ASCE 124–6: 630–634

Peirson W (1997) Measurement of surface velocities and shears at a wavy air-water interface using particle image velocimetry. Exp Fluids 23:427–437

Peregrine D, Svendsen L (1978) Spilling breakers, bores and hydraulic jumps. In: Proceedings of the 16th international conference on coastal engineering, 2nd edn., vol 1, pp 540–550

Phillips O (1961) A note on the turbulence generated by gravity waves. J Geophys Res 66–9:2889–2893

Rapp R, Melville W (1990) Laboratory measurements of deep water breaking waves. Philos Trans R Soc A 331:735–800

Reynolds O (1883) An experimental investigation of the circumstances which determine whether the motion of water shall be direct or sinuous, and of the law of resistance in parallel channels. Phil Trans R Soc Lond 174:935–982

Sheng J, Meng H, Fox R (2000) A large eddy PIV method for turbulence dissipation rate estimation. Chem Eng Sci 55: 4423–4434 (Pergamon-Elsevier Science Ltd)

Siddiqui K, Loewen M (2007) Characteristics of the wind drift layer and microscale breaking waves. J Fluid Mech 573:417–456

SPM84, Shore Protection Manual (1984) 4th edn., 2 vol. US Army Engineer Waterways Experiment Station US Government Printing Office, Washington, DC

Stokes G (1847) On the theory of oscillatory waves. Trans Cambr Philos Soc 8:441–455

Swan C (1990a) Wave kinematics within the crest to trough region. Environ Forces offshore Struct Predict 26:45–60

Swan C (1990b) Convection within an experimental wave flume. J Hydraul Res 28:273–282

Teixeira M, Belcher S (2002) On the distortion of turbulence by a progressive surface wave. J Fluid Mech 458:229–267

Tennekes H, Lumley J (1972) A first course in turbulence. 15th printing MIT Press Design Department, Cambridge

Terray E, Donelan M, Agrawal Y, Drennan W, Kahma K, Williams A III, Hwang P, Kitaigorodskii S (1996) Estimates of kinetic energy dissipation under breaking waves. J Phys Oceanogr 26: 792–807

Tolman H (2009) User manual and system documentation of WAVEWATCH III TM version 3.14. Technical note. MMAB Contribution No. 276. NOAA

Voulgaris G, Trowbridge J (1998) Evaluation of the acoustic Doppler velocimeter (ADV) for turbulence measurements. J Atmos Ocean Technol 15:272–289

Wiegel R (1964) Oceanographical engineering. Prentice Hall International in Theoretical and Applied Mechanics. N. M. Newmark editor, Englewood Cliffs